

The Carnegie RR Lyrae Program: The (Near- and??) Mid-Infrared RR Lyrae Period-Luminosity-Metallicity Relations in ω Cen

Meredith J. Durbin^{1,2} Victoria Scowcroft^{3,4} Wendy L. Freedman⁵ Barry F. Madore⁴
 Rachael L. Beaton⁴ Andrew J. Monson⁶ Jeffrey Rich Jr.⁴ Mark Seibert⁴

¹ Department of Astronomy, University of Washington, 3910 15th Ave NE, Seattle, WA 98105, USA

² Space Telescope Science Institute, 3700 San Martin Drive, Baltimore, MD 21218, USA

³ *MJD: I cannot find the address of the Bath astro department*

⁴ Observatories of the Carnegie Institution of Washington, 813 Santa Barbara St., Pasadena, CA 91101, USA

⁵ Department of Astronomy and Astrophysics, University of Chicago, 5640 S Ellis Ave, Chicago, IL 60637, USA

⁶ Department of Astronomy and Astrophysics, The Pennsylvania State University, 525 Davey Lab, University Park, PA, 16802, USA

Accepted XXX. Received YYY; in original form ZZZ

ABSTRACT

Key words: keyword1 - keyword2 - keyword3

1 INTRODUCTION

Given its proximity, size, and complexity, ω Centauri (NGC 5139) has become one of the most well-studied Galactic globular clusters (GGCs) (van Leeuwen et al. 2002). It has a mass of approximately $4 \times 10^6 M_\odot$ (D’Souza & Rix 2013), and a tidal radius of 88 pc (Mackey & van den Bergh 2005). ω Cen’s close proximity to Earth ($d \sim 5.5$ kpc, e.g. Del Principe et al. 2006; Thompson et al. 2001) allows us to resolve the stellar population of this dense cluster.

Although it has been subject to decades of investigations, the true nature of ω Cen remains unclear. It is one of the most massive GGCs orbiting the Milky Way. It is significantly flattened ($\epsilon = 1 - b/a = 0.17$ Mackey & van den Bergh 2005) and it does not show the levels of mass segregation in its stellar population that would be expected were it in equipartition (Anderson 2002). Additionally, ω Cen was the first GGC discovered to comprise more than one stellar population (Lee et al. 1999), breaking down the prevailing interpretation that GGCs were simple stellar populations with a single episode of star formation, hence a monolithic age and metallicity distribution.

There are at least seven distinct stellar populations in ω Cen (Tailo et al. 2016), with a spread in metallicity as large as 0.8 to 1.4 dex (Villanova et al. 2014; Marino et al. 2012; Johnson & Pilachowski 2010). As all the stars in ω Cen are at approximately the same distance from Earth¹, it is the

ideal testbed for studying the effects of changing metallicity on a population.

In this work we focus on the effects of changing metallicity on the RR Lyrae variables (RRL), specifically examining whether the period–luminosity (PL) relations in the near- and mid-infrared (IR) are affected, and the magnitude of any such effects. ω Cen has been used previously for such studies, ranging from empirical tests in the optical (e.g. Olech et al. 2003; Lee 1991) and near-IR (e.g. Cacciari et al. 2006; Del Principe et al. 2006), to semi-empirical tests using population synthesis techniques (Tailo et al. 2016).

This work is part of the Carnegie RR Lyrae Program (CRRP), a Warm *Spitzer* Exploration Science program with the aim of provide an independent, Population II anchor to the extragalactic distance scale. Tied to RR Lyrae variables with high-precision, geometric distances in the Milky Way, the CRRP will ultimately provide a single instrument measurement of H_0 , independent of Cepheid measurements, putting important constraints on the external accuracy of the standard candle distance ladder, and the internal consistency of the distance measurements of Cepheids and RR Lyrae variables.

Although observing RRL at mid-IR wavelengths dramatically reduces the effects of reddening and extinction ($A_{[3.6]} \sim A_V/16$ Indebetouw et al. 2005), a consensus has not been reached on the consequences of this shift to longer wavelengths on the metallicity term in the empirical RRL PL relation. Both theory and observation have demonstrated that the position of the horizontal branch in the optical colour–magnitude diagram is dependent on metallicity (e.g. Marconi et al. 2015; Catelan et al. 2004; Bono et al. 2003;

¹ In this case, the spread in distance due to the depth of the cluster is negligible.

Nemec et al. 1994). However, the size of the metallicity contribution in the infrared PL relation is yet to be settled in the literature, either from a theoretical or empirical standpoint.

The most in-depth study of the effect of metallicity on the mid-IR PL relation to date comes from Dambis et al. (2014), who used WISE data (Wright et al. 2010; Cutri et al. 2013) to examine possible changes in the RRL PL relation in globular clusters with different metallicities. They found a moderate metallicity dependence of the [W1]² PL relation, with $\gamma_{W1} = 0.106 \pm 0.023 \text{ mag dex}^{-1}$, slightly larger than their value for the near-IR, and approximately half that of the optical dependence ($\gamma_K = 0.088 \pm 0.026 \text{ mag dex}^{-1}$, $\gamma_V = 0.232 \pm 0.020 \text{ mag dex}^{-1}$, Dambis et al. 2013). The observational work of Muraveva et al. (2015) appears to confirm this result, favouring a low value of γ_K for Milky Way and Large Magellanic Cloud RRL. However, the empirical study of Karczmarek et al. (2015) considers near-IR observations of RRL in the Carina dwarf Spheroidal (dSph) galaxy, this time testing different PL relations with a range of metallicity coefficients. Their results favour a larger value for γ_K than Dambis et al. (2015), with average values of $\gamma_K \approx 0.18 \text{ mag dex}^{-1}$. This is consistent with the theoretical models by Marconi et al. (2015), who find that the metallicity dependence of the infrared PL relation is just as large as at optical wavelengths.

Our study is unique as it is the first study to use ω Cen to empirically measure the metallicity effect on the mid-IR RRL PL relation using metallicities of individual stars, rather than comparing the populations of RRL in different GGCs or dSph. Our approach — studying only *differential photometric effects* — removes the systematic uncertainties introduced by comparing populations at different distances with different levels of foreground extinction, and in some cases observed with different instruments.

The paper is set out as follows: Section 2 details the observations and data reduction. Section 3 presents the photometry of the ω Cen RRL. Section 4 describes the mid-IR PL relations and Section ?? discusses the application of these to a distance measurement of ω Cen. Section 5 examines the effects of metallicity on RRL magnitudes and distance estimates. Section 6 discusses the implications of this, and other systematic effects we consider in this work. In Section 7 we present our conclusions.

2 OBSERVATIONS & DATA REDUCTION

This work combines mid-IR observations from the CRRP Warm *Spitzer* program with supporting near-IR observations from the FourStar instrument (Persson et al. 2013) on the Baade-Magellan telescope at Las Campanas Observatory. Figure 1 shows a K_s -band FourStar image with the *Spitzer* fields outlined, and the positions of known RRL from Kaluzny et al. (2004) indicated by circles (fundamental mode, RRab) or triangles (first overtone, RRc).

² approximately equivalent to *Spitzer* 3.6 μm band

2.1 Spitzer Data

The *Spitzer* observations for this work were taken as part of the CRRP Freedman et al. (2012, *Spitzer* PID 90002). Three fields in ω Cen were chosen; their positions are shown in Figure 1. To obtain optimal RRL light curves we observed each field 12 times over approximately 16 hours (0.67 days), roughly corresponding to the longest period RRL we expected in the field and ensuring full phase coverage of all RRL. The observations of all three fields were taken on 2013 May 10 and 2013 May 11. Each field was observed using the *Spitzer* InfraRed Array Camera (IRAC) (Fazio et al. 2004) with a 30 s frame time with a medium scale, gaussian 5-point dither pattern to mitigate any image artefacts. Images were collected in both the 3.6 and 4.5 μm channels. The elongated field shapes come from the design of IRAC; while the [3.6] channel is collecting on-target data, the [4.5] channel collects off target data “for free”, and vice versa. We chose to include these off-target fields to maximise the number of RRL in our final sample and to increase the legacy value of our data set to the community.

The science images were created using MOPEX (Makovoz et al. 2006), first running overlap correction on the corrected basic calibrated data frames (cBCDs) then mosaicking the original, under-sampled 1.2 arcsec scale images to a scale of 0.6 arcsec/pixel using the drizzle algorithm. Mosaicked location-correction images were created at the same time. The science mosaics have a signal to noise of approximately 100 at the brightness level of the RRL in both bands.

PSF photometry was performed on the mosaicked images using DAOPHOT and ALLFRAME (Stetson 1987, 1994). The PSF model was created for each field/filter combination using the first epoch data and was applied to every epoch. As the observations were taken temporally close together the effects of telescope rotation between epochs on the mosaicked PSF were minimal, so making a single good PSF model for each field/filter combination proved to be more efficient and just as accurate as creating one for every epoch.

Master star lists for ALLFRAME were created for each filter/field combination using a median mosaicked image created by MOPEX. We did not use the same single master star list for both filters as only a small proportion (1/3) of the [3.6] and [4.5] fields overlap each other. Instead we performed separate ALLFRAME reductions for each filter, and combined the results after the fact using DAOMATCH and DAOMASTER. Our mid-IR photometry is calibrated to the standard system set by Reach et al. (2005).

2.2 FourStar Data

J , H and K_s data were taken with the FourStar instrument on the Baade-Magellan telescope at Las Campanas Observatory (Persson et al. 2013) on the nights of 2013 June 25, 2013 June 27, and 2013 June 28. Four epochs were obtained each night in each filter for a total of 12 epochs, with a typical image quality of FWHM = 0.6 arcseconds in the K_s band. A mosaic of 5×3 slightly overlapping pointings (tiles), each with FourStar’s native 10.9×10.9 arc-minute field of view, covered a 50×30 arc-minute field of view centred on ω Cen. Each tile consists of a 5 point dither pattern with a 5.8 second exposure time. Stacked mosaics of the entire field were

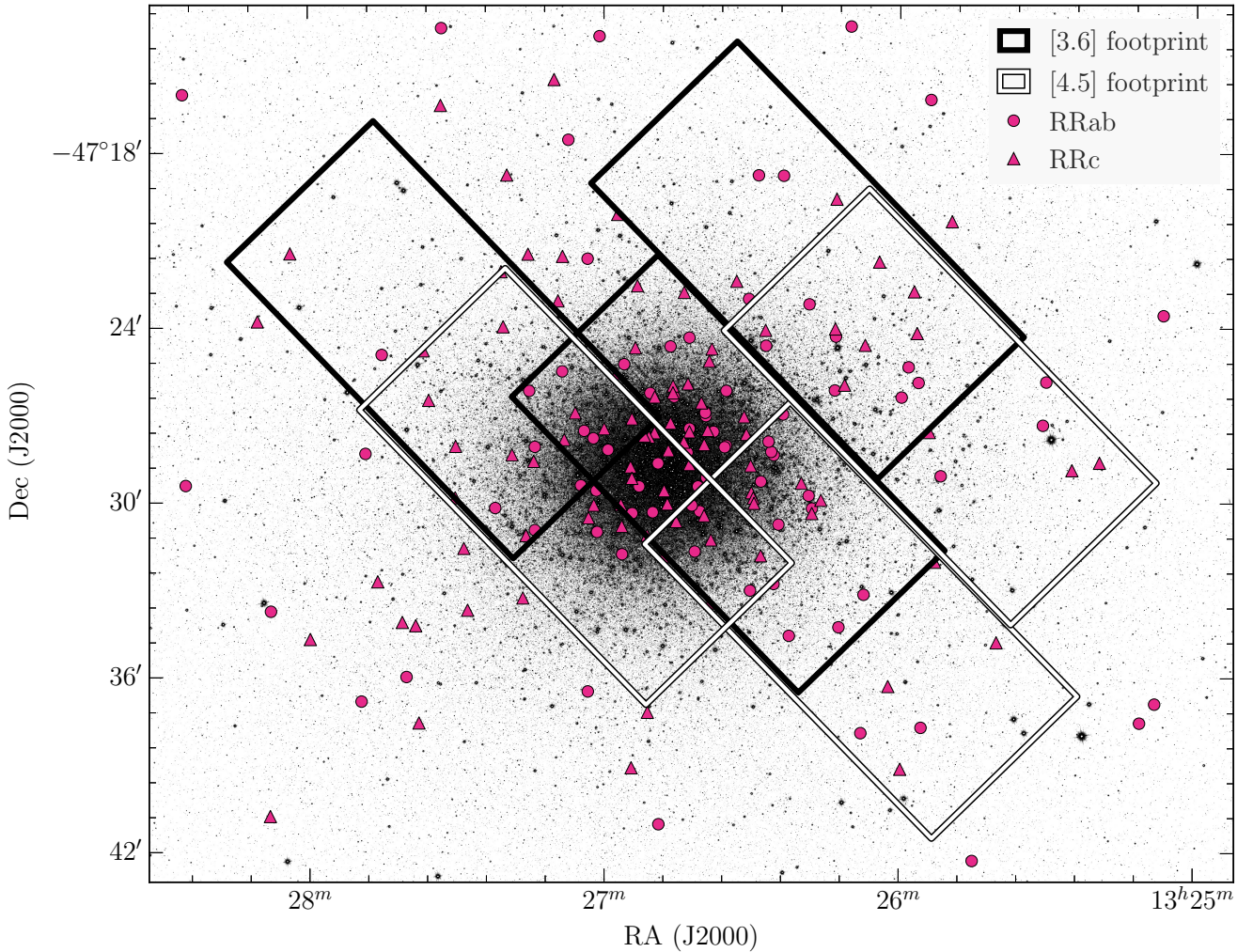


Figure 1. A K_s -band image of ω Cen from the FourStar camera, overlaid with a catalog of RRL from Kaluzny et al. (2004) and footprints of the *Spitzer* IRAC fields. The circular points are RRab's and the triangular points are RRc's; we adopt this convention throughout the paper. The three black rectangle outlines are the IRAC field of view for each pointing in the $3.6\ \mu\text{m}$ channel, and the white rectangle outlines show the same for $4.5\ \mu\text{m}$.

made as well as individual tiles using a customised pipeline for FourStar data. The purpose of the individual tiles is to provide photometry with better time resolution than the large mosaic.

PSF photometry of the tiles was performed using DAOPHOT and ALLFRAME (Stetson 1987, 1994). A PSF model was created for each epoch/tile/filter combination. A master star list for ALLFRAME was created from the final K_s mosaic and the multi-wavelength/epoch results were combined using DAOMATCH and DAOMASTER. Our final photometry is calibrated to the 2MASS standard system (Skrutskie et al. 2006).

2.3 Crowding

VS: Expand this section to include the crowded/uncrowded image cutouts.

MJD: Finally done...except now I can't remember whether these are actually relevant with the new way of rejecting

stuff.

3 RESULTS

Our final photometry catalog, including magnitudes and uncertainties for JHK_s , [3.6], and [4.5], is presented in Table A1.

4 PERIOD-LUMINOSITY RELATIONS

We fit PL relations of the form

$$m = a \times (\log P - \langle \log P \rangle) + b, \quad (1)$$

where $\langle \log P \rangle$ is the average of the logarithms of the periods in the sample. For our sample of RRab in ω Cen, $\langle \log P \rangle = -0.190$ days, and for RRc $\langle \log P \rangle = -0.450$ days. We use a simple linear least-squares fit unweighted by photometric

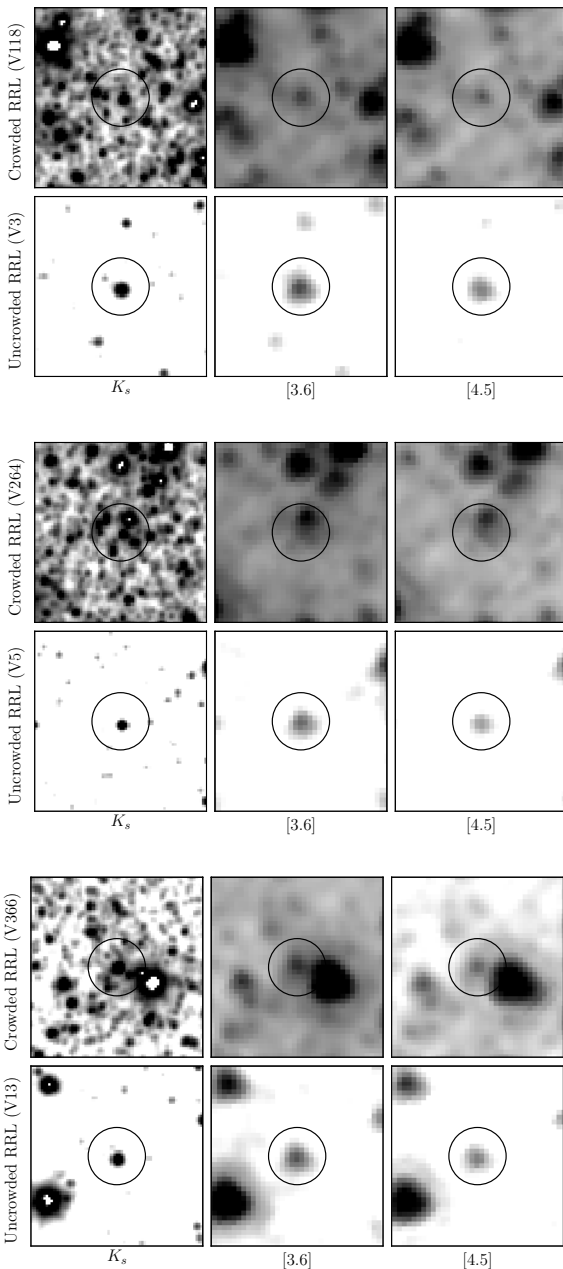


Figure 2. Three examples of crowded vs. uncrowded RRL, shown in K_s , [3.6], and [4.5]. Images are shown at the same color scale per filter with a log stretch. The RRL are circled.

errors to fit this relation to our photometry, and report the parameters a and b as well as the dispersion σ in Table 1.

The fitted PL relations for all five bands are shown in Figure 4. Coloured points (purple, blue, green, yellow, red) represent the J , H , K_s , [3.6], and [4.5] data that was included in the PL fits. Grey points represent stars that were excluded from the fits due to falling outside the 2σ clipping boundaries.

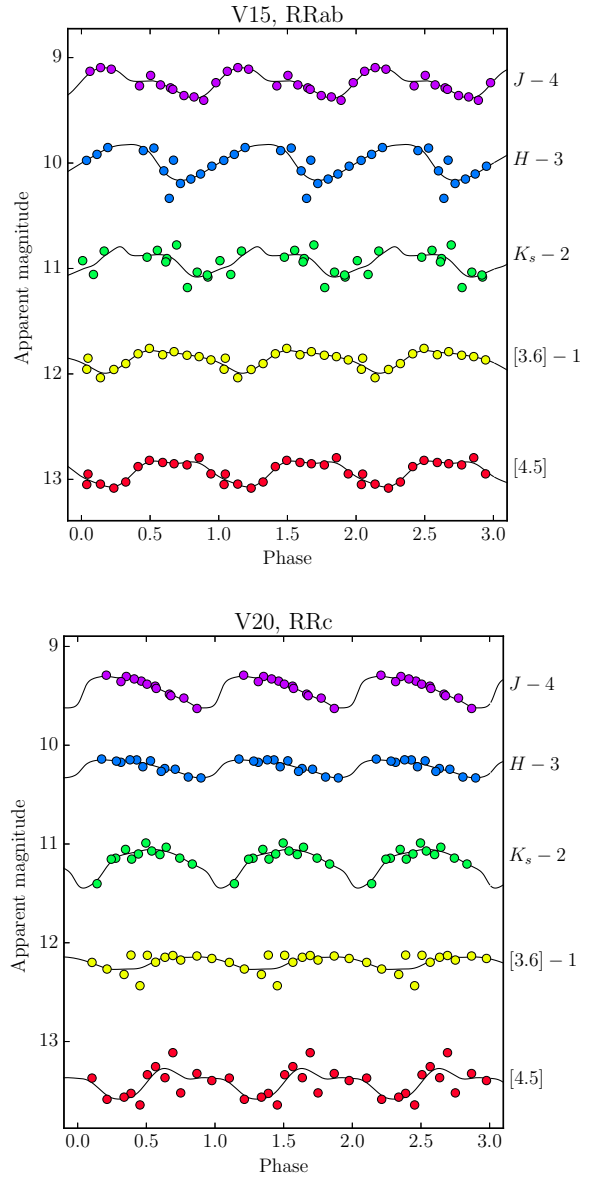


Figure 3. Sample phased JHK_s and IRAC light curves for two RRL, V15 and V20. The light curves were fit using GLOESS, a Gaussian local estimation algorithm which has been used throughout the CRRP.

5 METALLICITY

In principle, moving from the optical to the mid-infrared in uncrowded systems should bring the advantage of a steeper PL relation with decreased dispersion. However, theoretical works suggest that the metallicity coefficient in the infrared PL relations should be comparable to the metallicity coefficient at optical wavelengths (Bono et al. 2001; Catelan et al. 2004; Marconi et al. 2015). ω Cen is ideal for assessing the contribution of metallicity to the mid-IR RRL PL relation, because it is known to have a large spread in metallicity ($0.8 \leq \Delta [\text{Fe}/\text{H}] \leq 1.4$ dex Villanova et al. 2014; Marino et al. 2012; Johnson & Pilachowski 2010). A metal-

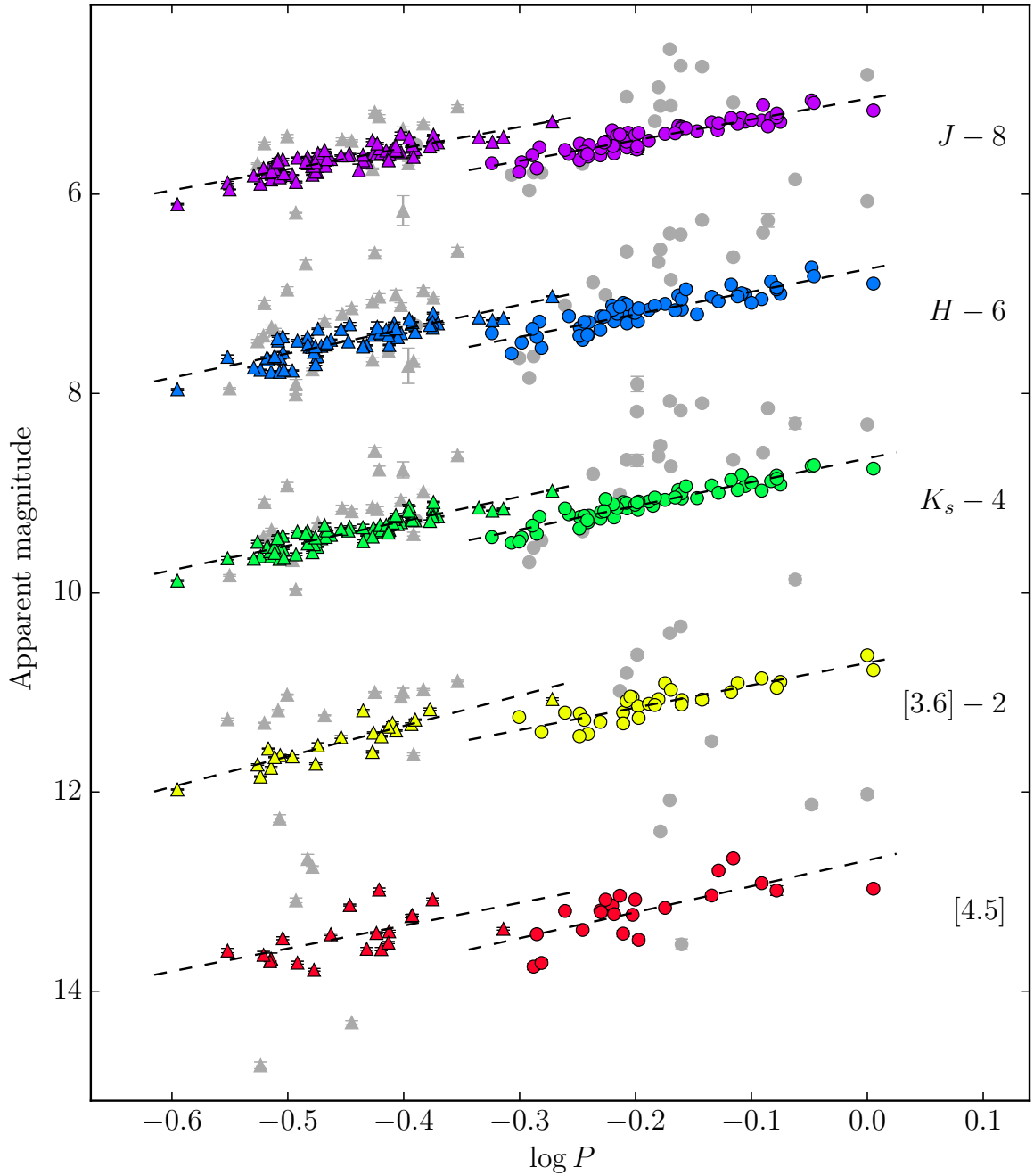


Figure 4. PL relations for JHK_s , [3.6], and [4.5] photometry. Here circles represent RRab stars and triangles represent RRc's. Coloured points are stars used in the PL fits, and grey points are stars rejected based on 2σ clipping.

licity spread this wide is not found in any other Galactic globular cluster.

One of the advantages of using globular clusters to calibrate PL coefficients is that all stars in a cluster can be considered to be at the same distance. The dispersion in the PL relation is a combination of the a) the intrinsic dispersion of the PL relation, b) the photometric uncertainties, and c) dispersion induced by other complicating factors such as the spread in metallicity. Since we have a measured ‘intrinsic’

dispersion of the RRL PL in [3.6] and [4.5] from the cluster M4 (Neeley et al. 2015) and the photometric uncertainties are well understood, we can isolate the remaining scatter due to astrophysical sources such as metallicity.

It has been shown with mid-IR spectra that a significant CO feature sits within the IRAC [4.5] filter. In the case of Cepheids, Scowcroft et al. (2016) have shown that this has a significant effect on the [4.5] magnitudes, and is metallicity dependent. However, this effect decreases with increasing

Table 1. Empirical ω Cen RRL period-luminosity relation coefficients for relations of the form $m = a + b \times (\log P - \langle \log P \rangle)$ (Eqn. 1) with observed dispersion σ .

Band	Mode	a	b	σ
<i>J</i>	RRab	-2.085 ± 0.114	13.438 ± 0.008	0.063
	RRc	-2.119 ± 0.129	13.644 ± 0.008	0.068
<i>H</i>	RRab	-2.269 ± 0.160	13.184 ± 0.012	0.086
	RRc	-2.440 ± 0.184	13.478 ± 0.011	0.088
K_s	RRab	-2.388 ± 0.110	13.106 ± 0.008	0.060
	RRc	-2.458 ± 0.132	13.406 ± 0.008	0.067
[3.6]	RRab	-2.247 ± 0.231	13.132 ± 0.017	0.090
	RRc	-3.058 ± 0.316	13.491 ± 0.022	0.096
[4.5]	RRab	-2.605 ± 0.558	13.183 ± 0.040	0.181
	RRc	-2.293 ± 0.732	13.458 ± 0.043	0.177

temperatures, turning off completely above 6000 K where all the CO has been destroyed (Scowcroft et al. 2016). As even the coolest RRL have temperatures over 6000 K (Iben 1971), we expect to see no such CO absorption affecting the [4.5] PL relation, nor do we expect any other temperature dependent (hence period dependent) metallicity effects. However, we can directly and empirically test this prediction.

5.1 Metallicity Contribution to the Overall Dispersion

We can place an upper limit on the contribution of astrophysical sources of scatter (e.g. metallicity, mass spread, evolutionary effects) to the observed ω Cen PL dispersion using the known variances of the individual components: the observed distribution of ω Cen PL residuals $\sigma_{\text{observed}}^2$, the intrinsic PL width $\sigma_{\text{intrinsic}}^2$, and the dispersion induced by photometric error σ_{phot}^2 . The dispersions contributed by astrophysical sources and by metallicity specifically can therefore be constrained as follows:

$$\sigma_{\text{astro}} \leq \sqrt{\sigma_{\text{observed}}^2 - \sigma_{\text{intrinsic}}^2 - \sigma_{\text{phot}}^2} \quad (2)$$

$$\sigma_{[\text{Fe}/\text{H}]} \leq \sigma_{\text{astro}} \quad (3)$$

MJD: OKAY how are we doing this? Are we using Reticulum or M4? If M4, do we have updated photometry from Neeley? If Reticulum, there are 3 band-pulsation mode combinations where average photometric error exceeds observed scatter so that's awkward

Table 2 shows the estimated contribution to the dispersion from metallicity $\sigma_{[\text{Fe}/\text{H}]}$ in each band, alongside the contributions from the photometric uncertainties and intrinsic components (from Marconi et al. 2015; Neeley et al. 2015, for the near- and mid-IR, respectively).

We use these estimates of $\sigma_{[\text{Fe}/\text{H}]}$ to assess the γ parameter for ω Cen, where

$$\gamma = \frac{\Delta \text{mag}}{\Delta [\text{Fe}/\text{H}]} \text{ mag dex}^{-1}, \quad (4)$$

similar to γ used to quantify the effect of metallicity on the zero-point of the Cepheid PL relation (Kennicutt et al. 1998; Scowcroft et al. 2009). Here we calculate γ in units of mag dex^{-1} by dividing the standard deviation of the metallicity component of the PL scatter by the standard deviation of the metallicity distribution

Table 2. The standard deviation of the observed spread of the PL residuals σ_{observed} (σ in Table 1) and its components: $\sigma_{\text{intrinsic}}$, σ_{phot} , and $\sigma_{[\text{Fe}/\text{H}]}$ for all PL relations. MJD: NEEDS UPDATING, assuming we're still doing this bit

Band	Mode	σ_{observed}	$\sigma_{\text{intrinsic}}$	σ_{phot}	$\sigma_{[\text{Fe}/\text{H}]}$
<i>J</i>	RRab	0.127	0.060	0.018	0.111
	RRc	0.082	0.040	0.015	0.070
<i>H</i>	RRab	0.170	0.040	0.028	0.163
	RRc	0.107	0.020	0.024	0.102
K_s	RRab	0.147	0.030	0.023	0.142
	RRc	0.089	0.020	0.021	0.084
[3.6]	RRab	0.124	0.040	0.052	0.106
	RRc	0.096	0.079	0.044	0.034
[4.5]	RRab	0.154	0.045	0.046	0.140
	RRc	0.219	0.057	0.054	0.205

It is important to note that these values presented in Tables 2 and ?? are upper limits, and as we will show in Sections 5.2 and 6, the size of the effect that can be attributed to metallicity effects alone may be much smaller.

5.2 PL Residuals and Individual Metallicities

ω Cen provides a second approach to testing for a metallicity effect on the RRL PL relation. The cluster is well studied and many of its RRL have metallicity measurements in the literature (e.g. Sollima et al. 2006; Rey et al. 2000; Braga et al. 2016). Braga et al. (2016) in particular provide several measurements of RRL metallicities, including revisions of metallicities from Sollima et al. (2006) and Rey et al. (2000) scaled to the homogeneous cluster metallicity scale described in Carretta et al. (2009), and new estimates based on the residuals of the *I*-band PL relation. Here we choose to use their weighted average of the rescaled Sollima et al. (2006) and Rey et al. (2000) metallicities to avoid any potential degeneracies caused by using metallicities calculated based on PL residuals.

Theory predicts a linear metallicity term in the PLZ relation in the optical and infrared, $c \times [\text{Fe}/\text{H}]$. We thus fit a relation of the form

$$\Delta \text{mag} = \gamma \times [\text{Fe}/\text{H}] + d \quad (5)$$

to the PL residuals and metallicity values for stars with known metallicity values, as shown in Figures 5, 6, 7, 8, and 9. The scatter in the [3.6] and [4.5] PL relations is higher for ω Cen than it is for M4 (Neeley et al. 2015; Braga et al. 2015); however, when we examine $[\text{Fe}/\text{H}]$ vs. the residuals of each PL relation, γ is within 2σ of zero for all fits, indicating that there is no significant metallicity dependence in the PL residuals. The flatness of these relations hints that the source of additional dispersion in the ω Cen PL relations may not be due to metallicity, but in fact due to other evolutionary effects such as the spread in age of its multiple populations. This is discussed further in Section 6.

Based on the γ measurements we find here, there is no evidence for a metallicity dependence in any band. Even taking our most extreme γ value, the maximum change in magnitude due to metallicity for a 1.2 dex $[\text{Fe}/\text{H}]$ spread would be $0.172 \times 1.2 = 0.21$ mag, which is comparable to the observed scatter of the PL relation in [4.5].

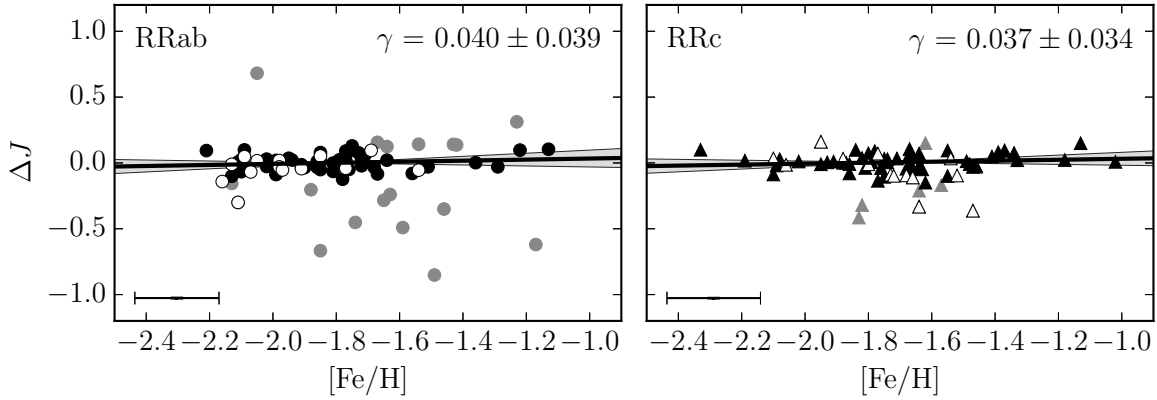


Figure 5. [Fe/H] values (Braga et al. 2016) vs. period-luminosity residuals (Δmag) for RRab (left) and RRc (right) in J . Filled black points are stars included in the fit, filled grey points are stars rejected from the PL fit by 2σ clipping, and open points are stars with metallicity errors greater than 0.3 dex. Solid lines are the line of best fit with slope γ , and the grey space represents the 2σ confidence intervals of the fit. The crossed lines at the bottom left corner of each subplot represent average errors in [Fe/H] and Δmag . The γ parameter from equation 4 is shown in the top right corner of each plot. All γ values are consistent with zero within 2σ , and most are consistent within 1σ .

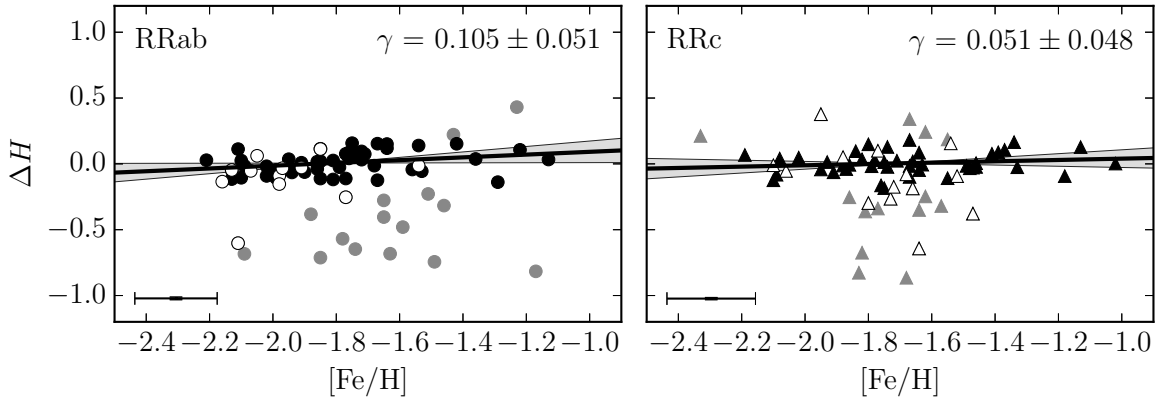


Figure 6. Same as Figure 5, but for H .

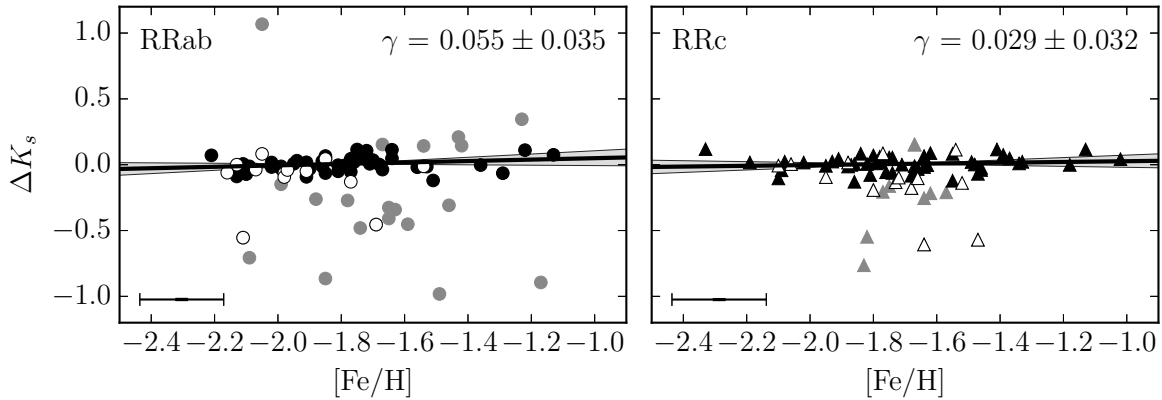
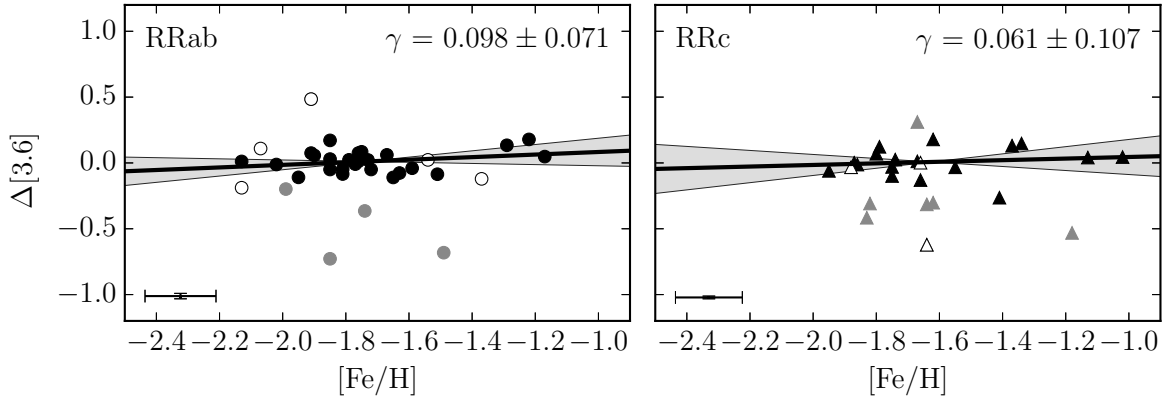
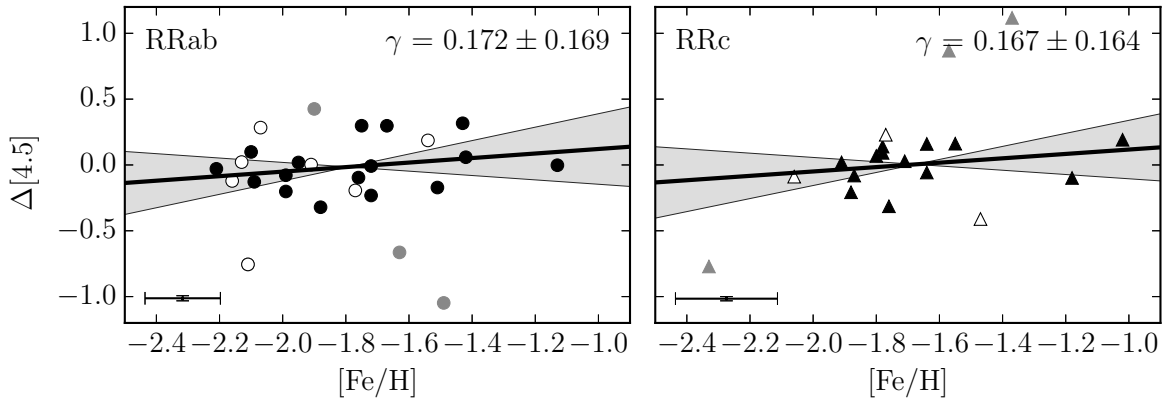


Figure 7. Same as Figure 5, but for K_s .

**Figure 8.** Same as Figure 5, but for [3.6].**Figure 9.** Same as Figure 5, but for [4.5].

6 DISCUSSION

6.1 Evolutionary Effects

While we find high upper bounds on the contribution of metallicity to the PL scatter in all infrared passbands, it is unlikely that this scatter is due to metallicity alone. [Gratton et al. \(1986\)](#) and [Lee \(1991\)](#) demonstrate that RRL luminosity is dependent on the horizontal branch morphology as well as metallicity; it is also well known that ω Cen contains RRLs in multiple evolutionary states ([Sollima et al. 2008](#); [Navarrete et al. 2015](#)). [Marconi et al. \(2015\)](#) performed extensive theoretical studies of the effects of both RRL composition and evolutionary state on the position of the horizontal branch in the Hertzsprung–Russell (HR) diagram. In their figure 2 they present the HR diagram for a selection of models at a fixed composition for a range of evolutionary states, demonstrating a spread in 0.3 dex in bolometric luminosity between the least evolved, zero-age horizontal branch (ZAHB) mass RRL and the most evolved RRL. The RRL population in ω Cen is thought to be comprised of (at least) two different populations — the metal rich population being the less evolved ZAHB phase stars, with the more metal

poor population in an advanced evolutionary state ([Tailo et al. 2016](#)). This spread in evolutionary state *in addition to* the spread in metallicity could create the additional dispersion observed in the ω Cen PL relations.

6.2 Improvements to the Mid-IR PL Calibration

We note here a concern with the current adopted slopes for RRab and RRc variables at $4.5\ \mu\text{m}$ from [Neeley et al. \(2015\)](#) (and to a lesser degree for the corresponding slopes for the $3.6\ \mu\text{m}$ PL relations). There are two indications that the slopes may not be correct. First, we note that the slope of the respective PL relations as a function of wavelength is not monotonically increasing with increasing wavelength, as expected as the slope asymptotically approaches the slope of the wavelength-independent period-radius relation. For the RRab variables a relatively smooth trend is observed. However, for the RRc variables the situation is less clear. While the three near-infrared slopes follow the RRab trend in lock-step, the slope at $3.6\ \mu\text{m}$ is very shallow with respect to the value expected from a smooth extrapolation from the

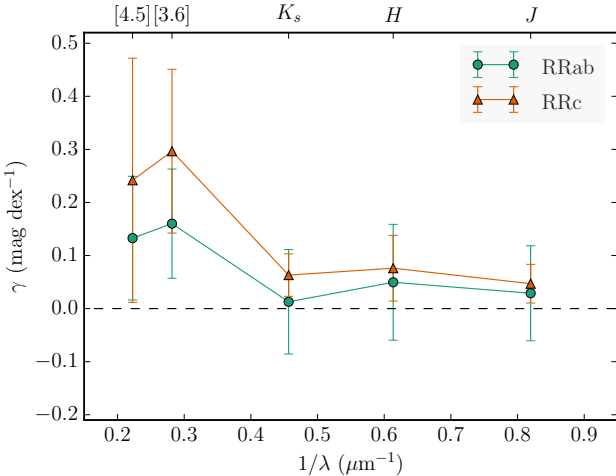


Figure 10. Metallicity slope dependence on wavelength. At each of five wavelengths along the x axis (corresponding to the J , H , K_s , 3.6 and 4.5 μm bandpasses) we plot on the y axis the results of a regression of magnitude residuals against metallicities, searching both for a signal and for any trend in that signal with wavelength. Neither trend is found. Colour-coded symbols break the data down into RRab and RRc type variables (circles and triangles, respectively). Virtually all of the individual data points are consistent with no metallicity effect on the observed magnitudes, independent of wavelength and RRL type.

shorter wavelengths, and then at 4.5 μm the slope becomes unexpectedly large. This pattern of behaviour is unphysical.

Future data, beyond the scope of this paper, will be required to improve upon these slopes; however, we note that the slopes at 3.6 μm and 4.5 μm should both be around -2.80 , suggesting that 3.6 μm will be steeper by 0.09 (a 5% adjustment) and that the slope at 4.5 μm will be flatter by 0.18 (an 6% adjustment). Second, the correspondence of the 3.6 and 4.5 μm magnitude residuals from their respective PL relations would be made tighter if the 4.5 μm PL relation for the RRc variables were made shallower, or the 3.6 μm slope made steeper, or both, as suggested above.

The issue of whether this difference in slope is due to differences in metallicity between ω Cen and M4 (the calibrating sample in Neeley et al. 2015), or to another effect such as the discrepant period distributions of the samples, or a difference in analysis technique, requires an independent sample of RRL at a single metallicity, and as such cannot be answered with the ω Cen sample.

MJD: Well uh. Do we want to say anything about GAIA now? Results from the Gaia mission (Lindegren & Perryman 1996) are expected to improve the overall characterisation of the RRL PL relation dramatically. Trigonometric parallaxes and spectrophotometric metallicities of Galactic RRLs from Gaia will increase the number of high quality calibrators for the infrared PL relations by an order of magnitude (Liu et al. 2012, Scowcroft et al. 2016b, in prep., Beaton et al. 2016, in prep.).

In addition to the calibration of the slope and absolute zero-point of the RRL PL relation, Gaia will also provide important insights regarding ω Cen. Gaia will observe many of the RRL in ω Cen (Babusiaux et al. 2002), providing

0.2% parallaxes and spectrophotometric metallicities for the individual stars. Combining the photometric data presented here with the Gaia sample of high-quality parallaxes and consistent metallicities we will be able to further constrain the effect on the mid-IR PL relation.

We also anticipate that the NIRCam instrument on *JWST* (Burriesci 2005; Gardner et al. 2006) will provide substantial improvements over IRAC for investigations of this nature. The NIRCam filters F356W and F444W will provide data in passbands comparable to IRAC's [3.6] and [4.5] at an order of magnitude higher resolution (0.065 arcsec/pixel), which will significantly decrease photometric error due to crowding and therefore allow us to obtain data for the full sample of RRL in ω Cen. With the parallaxes and differential metallicities from Gaia, and the high precision photometry from *JWST*, studies of ω Cen will allow us to explore the effects of metallicity and evolutionary effects on the RRL populations of globular clusters.

7 CONCLUSIONS

We derive a mean dereddened distance modulus for ω Cen of $\langle \mu_0 \rangle = 13.743 \pm 0.026$ with reddening $E(B-V) = 0.138 \pm 0.044$ using distance moduli derived from RRab PL relations in JHK_s , [3.6], and [4.5]. Using the mean of RRab and RRc distance moduli in the same passbands, we derive a mean dereddened distance modulus of $\langle \mu_0 \rangle = 13.789 \pm 0.018$ with reddening $E(B-V) = 0.084 \pm 0.030$. The value found using RRab alone is in better agreement with those in the literature (e.g. Lub 2002; Del Principe et al. 2006).

We also constrain the contribution of metallicity on the dispersion of the RRL PL relations by considering the variances associated with each component of the PL relation. We find that at most metallicity contributes 0.106 and 0.140 mag in dispersion to the [3.6] and [4.5] RRab PL relations respectively. Converting these values into γ , the PL relation metallicity coefficient, we find high upper limits compared to theoretical predictions for all infrared wavelengths.

When deriving γ empirically using the residuals from the RRL PL relations and the individual metallicities of the stars, we find γ values consistent with zero at all infrared wavelengths. We thus conclude that the upper limits derived in Section 5.1 are likely a combination of metallicity and evolutionary effects due to the evolutionary spread of the populations in ω Cen.

ACKNOWLEDGEMENTS

We thank Eric Persson for his many contributions to this project.

This work is based on observations made with the Spitzer Space Telescope, which is operated by the Jet Propulsion Laboratory, California Institute of Technology under a contract with NASA. Support for this work was provided by NASA through an award issued by JPL/Caltech.

This work was also supported in part by the Claremont-Carnegie Astrophysics Research Program.

This publication makes use of data products from the Two Micron All Sky Survey, which is a joint project of the

University of Massachusetts and the Infrared Processing and Analysis Center/California Institute of Technology, funded by the National Aeronautics and Space Administration and the National Science Foundation.

This research has made use of the NASA/IPAC Extragalactic Database (NED), which is operated by the Jet Propulsion Laboratory, California Institute of Technology, under contract with the National Aeronautics and Space Administration.

This research made use of Astropy, a community-developed core Python package for Astronomy ([Astropy Collaboration et al. 2013](#)).

REFERENCES

- Anderson J., 2002, in van Leeuwen F., Hughes J. D., Piotto G., eds, Astronomical Society of the Pacific Conference Series Vol. 265, Omega Centauri, A Unique Window into Astrophysics. p. 87
- Astropy Collaboration et al., 2013, [A&A](#), **558**, A33
- Babusiaux C., van Leeuwen F., Gilmore G., 2002, in van Leeuwen F., Hughes J. D., Piotto G., eds, Astronomical Society of the Pacific Conference Series Vol. 265, Omega Centauri, A Unique Window into Astrophysics. p. 415
- Bono G., Caputo F., Castellani V., Marconi M., Storm J., 2001, [MNRAS](#), **326**, 1183
- Bono G., Caputo F., Castellani V., Marconi M., Storm J., Degl'Innocenti S., 2003, [MNRAS](#), **344**, 1097
- Braga V. F., et al., 2015, [ApJ](#), **799**, 165
- Braga V. F., et al., 2016, preprint, ([arXiv:1609.04916](#))
- Burriesci L. G., 2005, in Heaney J. B., Burriesci L. G., eds, Proc. SPIE Vol. 5904, Cryogenic Optical Systems and Instruments XI. pp 21–29, doi:[10.1117/12.613596](#)
- Cacciari C., Sollima A., Ferraro F. R., 2006, Mem. Soc. Astron. Italiana, **77**, 245
- Carretta E., Bragaglia A., Gratton R., D'Orazi V., Lucatello S., 2009, [A&A](#), **508**, 695
- Catelan M., Pritzl B. J., Smith H. A., 2004, [ApJS](#), **154**, 633
- Cutri R. M., et al., 2013, Technical report, Explanatory Supplement to the AllWISE Data Release Products
- D'Souza R., Rix H.-W., 2013, [MNRAS](#), **429**, 1887
- Dambis A. K., Berdnikov L. N., Kniazev A. Y., Kravtsov V. V., Rastorguev A. S., Sefako R., Vozyakova O. V., 2013, [MNRAS](#), **435**, 3206
- Dambis A. K., Rastorguev A. S., Zabolotskikh M. V., 2014, [MNRAS](#), **439**, 3765
- Dambis A. K., Berdnikov L. N., Kniazev A. Y., Kravtsov V. V., Rastorguev A. S., Sefako R., Vozyakova O. V., Zabolotskikh M. V., 2015, [Publication of Korean Astronomical Society](#), **30**, 183
- Del Principe M., et al., 2006, [ApJ](#), **652**, 362
- Fazio G. G., et al., 2004, [ApJS](#), **154**, 10
- Freedman W., et al., 2012, The Carnegie RR Lyrae Program, Spitzer Proposal
- Gardner J. P., et al., 2006, [Space Sci. Rev.](#), **123**, 485
- Gratton R. G., Tornambe A., Ortolani S., 1986, [A&A](#), **169**, 111
- Iben Jr. I., 1971, [PASP](#), **83**, 697
- Indebetouw R., et al., 2005, [ApJ](#), **619**, 931
- Johnson C. I., Pilachowski C. A., 2010, [ApJ](#), **722**, 1373
- Kaluzny J., Olech A., Thompson I. B., Pych W., Krzeminski W., Schwarzenberg-Czerny A., 2004, [A&A](#), **424**, 1101
- Karczmarek P., et al., 2015, [AJ](#), **150**, 90
- Kennicutt Jr. R. C., et al., 1998, [ApJ](#), **498**, 181
- Lee Y.-W., 1991, [ApJ](#), **373**, L43
- Lee Y.-W., Joo J.-M., Sohn Y.-J., Rey S.-C., Lee H.-C., Walker A. R., 1999, [Nature](#), **402**, 55
- Lindgren L., Perryman M. A. C., 1996, [A&AS](#), **116**, 579
- Liu C., Bailer-Jones C. A. L., Sordo R., Vallenari A., Borrachero R., Luri X., Sartoretti P., 2012, [MNRAS](#), **426**, 2463
- Lub J., 2002, in van Leeuwen F., Hughes J. D., Piotto G., eds, Astronomical Society of the Pacific Conference Series Vol. 265, Omega Centauri, A Unique Window into Astrophysics. p. 95
- Mackey A. D., van den Bergh S., 2005, [MNRAS](#), **360**, 631
- Makovoz D., Roby T., Khan I., Booth H., 2006, in Society of Photo-Optical Instrumentation Engineers (SPIE) Conference Series. p. 62740C, doi:[10.1117/12.672536](#)
- Marconi M., et al., 2015, [ApJ](#), **808**, 50
- Marino A. F., et al., 2012, [ApJ](#), **746**, 14
- Muraveva T., et al., 2015, [ApJ](#), **807**, 127
- Navarrete C., et al., 2015, [A&A](#), **577**, A99
- Neeley J. R., et al., 2015, [ApJ](#), **808**, 11
- Nemec J. M., Nemec A. F. L., Lutz T. E., 1994, [AJ](#), **108**, 222
- Olech A., Kaluzny J., Thompson I. B., Schwarzenberg-Czerny A., 2003, [MNRAS](#), **345**, 86
- Persson S. E., et al., 2013, [PASP](#), **125**, 654
- Reach W. T., et al., 2005, [PASP](#), **117**, 978
- Rey S.-C., Lee Y.-W., Joo J.-M., Walker A., Baird S., 2000, [AJ](#), **119**, 1824
- Scowcroft V., Bersier D., Mould J. R., Wood P. R., 2009, [MNRAS](#), **396**, 1287
- Scowcroft V., Seibert M., Freedman W. L., Beaton R. L., Madore B. F., Monson A. J., Rich J. A., Rigby J. R., 2016, [MNRAS](#), **459**, 1170
- Skrutskie M. F., et al., 2006, [AJ](#), **131**, 1163
- Sollima A., Borissova J., Catelan M., Smith H. A., Minniti D., Cacciari C., Ferraro F. R., 2006, [ApJ](#), **640**, L43
- Sollima A., Ferraro F. R., Pancino E., Bellazzini M., 2008, Mem. Soc. Astron. Italiana, **79**, 342
- Stetson P. B., 1987, [PASP](#), **99**, 191
- Stetson P. B., 1994, [PASP](#), **106**, 250
- Tailo M., Di Criscienzo M., D'Antona F., Caloi V., Ventura P., 2016, [MNRAS](#), **457**, 4525
- Thompson I. B., Kaluzny J., Pych W., Burley G., Krzeminski W., Paczynski B., Persson S. E., Preston G. W., 2001, [AJ](#), **121**, 3089
- Villanova S., Geisler D., Gratton R. G., Cassisi S., 2014, [ApJ](#), **791**, 107
- Wright E. L., et al., 2010, [AJ](#), **140**, 1868
- van Leeuwen F., Hughes J. D., Piotto G., eds, 2002, Omega Centauri, A Unique Window into Astrophysics Astronomical Society of the Pacific Conference Series Vol. 265

APPENDIX A: RRL PHOTOMETRY

Table A1: Parameters for all RRL in ω Cen for which we have photometry in at least one band. The first four columns are the star ID, right ascension and declination, and pulsation mode from Kaluzny et al. (2004). Column 5 is the pulsation period in days from Braga et al. (2016). Columns 6 through 10 are apparent magnitudes and errors in JHK_s (FourStar) and [3.6] & [4.5] (IRAC). Columns 11 through 15 are the residuals from PL fitting for each band, where residual is defined as observed mag – predicted mag. Column 16 is the metallicity and error provided by Braga et al. (2016), which is a combination of metallicities from Rey et al. (2000) and Sollima et al. (2006) rescaled to the cluster metallicity scale provided by .

ID	RA (J2000)	Dec (J2000)	Mode	P (days)	<i>J</i> mag	<i>H</i> mag	<i>K_s</i> mag	[3.6] mag	[4.5] mag	ΔJ	ΔH	ΔK_s	$\Delta[3.6]$	$\Delta[4.5]$	[Fe/H]
V3	13:25:56.15	-47:25:53.8	RRab	0.841	13.275 ± 0.005	13.001 ± 0.005	12.915 ± 0.005	12.896 ± 0.020	...	0.077	0.078	0.084	0.023	...	-1.730 ± 0.050
V4	13:26:12.93	-47:24:18.8	RRab	0.627	13.499 ± 0.005	13.247 ± 0.006	13.143 ± 0.006	13.050 ± 0.013	13.233 ± 0.018	0.036	0.035	0.007	-0.110	0.019	-1.950 ± 0.050
V5	13:26:18.33	-47:23:12.4	RRab	0.515	13.783 ± 0.005	13.627 ± 0.006	13.549 ± 0.008	...	13.754 ± 0.031	0.141	0.222	0.210	...	0.317	-1.430 ± 0.170
V7	13:27:00.90	-47:14:00.5	RRab	0.713	13.369 ± 0.003	13.205 ± 0.009	13.051 ± 0.005	0.021	0.119	0.048	-1.640 ± 0.080
V8	13:27:48.45	-47:28:20.3	RRab	0.521	13.530 ± 0.004	13.279 ± 0.005	13.238 ± 0.004	-0.101	-0.115	-0.089	-2.130 ± 0.280
V9	13:25:59.58	-47:26:24.0	RRab	0.523	13.784 ± 0.005	13.543 ± 0.006	13.476 ± 0.005	13.398 ± 0.010	13.717 ± 0.030	0.157	0.153	0.153	0.061	0.297	-1.670 ± 0.060
V10	13:26:06.99	-47:24:36.6	RRc	0.375	13.585 ± 0.004	13.411 ± 0.007	13.351 ± 0.005	13.405 ± 0.007	...	-0.008	-0.007	0.005	-0.012	...	-1.860 ± 0.100
V11	13:26:30.59	-47:23:01.6	RRab	0.565	13.494 ± 0.004	13.341 ± 0.008	13.240 ± 0.007	13.214 ± 0.009	...	-0.065	0.026	-0.004	-0.048	...	-1.810 ± 0.150
V12	13:26:27.21	-47:24:06.2	RRc	0.387	13.597 ± 0.005	13.409 ± 0.008	13.313 ± 0.007	...	13.399 ± 0.011	0.033	0.024	0.000	...	0.028	-1.710 ± 0.140
V13	13:25:58.18	-47:25:21.6	RRab	0.669	13.395 ± 0.006	13.102 ± 0.006	13.069 ± 0.005	12.908 ± 0.017	13.163 ± 0.024	-0.011	-0.047	0.000	-0.188	0.022	-2.130 ± 0.500
V14	13:25:59.74	-47:39:09.6	RRc	0.377	13.597 ± 0.003	13.348 ± 0.006	13.384 ± 0.005	...	13.416 ± 0.011	0.010	-0.064	0.044	...	0.019	-1.910 ± 0.130
V15	13:26:27.11	-47:24:38.0	RRab	0.811	13.261 ± 0.005	13.054 ± 0.009	12.976 ± 0.007	12.860 ± 0.018	12.916 ± 0.024	0.030	0.095	0.106	-0.050	-0.008	-1.720 ± 0.070
V16	13:27:37.69	-47:37:34.8	RRc	0.330	13.688 ± 0.004	13.530 ± 0.006	13.442 ± 0.005	-0.022	-0.023	-0.040	-1.460 ± 0.050
V18	13:27:45.11	-47:24:56.6	RRab	0.622	13.384 ± 0.003	13.142 ± 0.007	13.115 ± 0.005	-0.088	-0.078	-0.030	-1.990 ± 0.280
V19	13:27:30.14	-47:28:05.2	RRc	0.300	13.895 ± 0.003	13.763 ± 0.005	13.634 ± 0.005	13.846 ± 0.007	14.743 ± 0.033	0.095	0.106	0.048	0.131	1.117	-1.370 ± 0.050
V20	13:27:14.05	-47:28:06.3	RRab	0.616	13.426 ± 0.004	13.217 ± 0.010	13.143 ± 0.007	13.201 ± 0.015	13.422 ± 0.030	-0.055	-0.013	-0.013	0.023	0.186	-1.540 ± 0.340
V21	13:26:11.17	-47:25:58.8	RRc	0.381	13.586 ± 0.005	13.404 ± 0.008	13.372 ± 0.006	13.441 ± 0.009	13.578 ± 0.017	0.008	0.002	0.042	0.045	0.191	-1.020 ± 0.110
V22	13:27:41.04	-47:34:07.6	RRc	0.396	13.579 ± 0.003	13.395 ± 0.005	13.292 ± 0.005	0.037	0.035	0.005	-1.820 ± 0.050
V23	13:26:46.50	-47:24:39.5	RRab	0.511	13.962 ± 0.007	13.845 ± 0.014	13.694 ± 0.010	0.312	0.431	0.345	-1.230 ± 0.050
V24	13:27:38.32	-47:34:14.5	RRc	0.462	13.428 ± 0.004	13.237 ± 0.004	13.145 ± 0.004	0.028	0.040	0.023	-2.080 ± 0.030
V25	13:26:25.52	-47:28:23.3	RRab	0.588	13.610 ± 0.006	13.361 ± 0.016	13.257 ± 0.010	13.298 ± 0.025	13.191 ± 0.014	0.089	0.086	0.055	0.075	-0.096	-1.760 ± 0.140
V26	13:26:23.64	-47:26:59.4	RRab	0.785	13.273 ± 0.005	13.008 ± 0.012	12.929 ± 0.008	0.012	0.017	0.026	-1.860 ± 0.040
V27	13:26:26.04	-47:28:16.5	RRab	0.616	13.451 ± 0.007	13.091 ± 0.017	13.090 ± 0.013	13.312 ± 0.017	...	-0.030	-0.139	-0.065	0.134	...	-1.290 ± 0.300
V30	13:26:15.94	-47:29:56.0	RRc	0.404	13.524 ± 0.006	13.299 ± 0.013	13.264 ± 0.009	13.319 ± 0.012	13.247 ± 0.017	0.001	-0.039	-0.001	0.001	-0.080	-1.870 ± 0.200
V32	13:27:03.32	-47:21:38.9	RRab	0.620	13.531 ± 0.003	13.297 ± 0.005	13.154 ± 0.005	0.057	0.075	0.007	-1.710 ± 0.160
V33	13:25:51.60	-47:29:05.8	RRab	0.602	13.359 ± 0.004	13.117 ± 0.006	13.117 ± 0.006	...	13.139 ± 0.021	-0.141	-0.135	-0.061	...	-0.121	-2.160 ± 0.440
V34	13:26:07.21	-47:33:10.4	RRab	0.734	13.278 ± 0.004	13.029 ± 0.004	12.923 ± 0.004	13.491 ± 0.032	13.040 ± 0.032	-0.043	-0.028	-0.049	0.485	0.003	-1.910 ± 0.500
V35	13:26:53.21	-47:22:34.7	RRc	0.387	13.593 ± 0.003	13.514 ± 0.007	13.367 ± 0.007	0.029	0.128	0.054	-1.740 ± 0.030
V36	13:27:10.11	-47:15:29.8	RRc	0.380	13.540 ± 0.002	13.389 ± 0.005	13.321 ± 0.004	-0.041	-0.016	-0.011	-1.670 ± 0.230
V38	13:27:03.30	-47:36:30.2	RRab	0.779	13.235 ± 0.004	12.994 ± 0.006	12.819 ± 0.005	-0.032	-0.004	-0.092	-1.910 ± 0.160
V39	13:27:59.77	-47:34:42.3	RRc	0.393	13.565 ± 0.003	13.435 ± 0.004	13.312 ± 0.004	0.017	0.068	0.017	-2.190 ± 0.290
V40	13:26:24.56	-47:30:46.2	RRab	0.634	13.544 ± 0.006	13.277 ± 0.015	13.169 ± 0.010	13.140 ± 0.017	...	0.090	0.076	0.045	-0.009	...	-1.770 ± 0.080
V41	13:27:01.41	-47:31:01.7	RRab	0.663	13.113 ± 0.020	12.555 ± 0.022	12.524 ± 0.031	...	12.397 ± 0.011	-0.300	-0.602	-0.554	...	-0.755	-2.110 ± 0.480
V44	13:26:22.39	-47:34:35.3	RRab	0.568	13.696 ± 0.004	13.450 ± 0.007	13.382 ± 0.005	0.142	0.139	0.143	-1.540 ± 0.110
V45	13:25:30.88	-47:27:21.0	RRab	0.589	13.540 ± 0.004	13.227 ± 0.004	13.188 ± 0.004	...	13.207 ± 0.012	0.019	-0.046	-0.013	...	-0.078	-1.990 ± 0.250
V46	13:25:30.23	-47:25:51.8	RRab	0.687	13.315 ± 0.005	13.017 ± 0.005	12.970 ± 0.004	-0.067	-0.106	-0.072	-2.100 ± 0.170
V47	13:25:56.46	-47:24:12.0	RRc	0.485	13.426 ± 0.006	13.244 ± 0.005	13.156 ± 0.005	...	13.374 ± 0.013	0.071	0.099	0.086	...	0.229	-1.770 ± 0.310
V49	13:26:07.78	-47:37:55.5	RRab	0.605	13.591 ± 0.003	13.276 ± 0.006	13.245 ± 0.005	...	13.227 ± 0.008	0.094	0.028	0.071	...	-0.029	-2.210 ± 0.110
V50	13:25:53.94	-47:27:35.8	RRc	0.386	13.656 ± 0.004	13.414 ± 0.004	13.374 ± 0.004	...	13.512 ± 0.010	0.090	0.027	0.059	...	0.139	-1.780 ± 0.190
V51	13:26:42.66	-47:24:21.4	RRab	0.574	13.622 ± 0.004	13.414 ± 0.009	13.293 ± 0.008	13.417 ± 0.021	...	0.079	0.115	0.066	0.171	...	-1.850 ± 0.020
V52	13:26:35.19	-47:28:03.8	RRab	0.660	12.926 ± 0.007	12.681 ± 0.016	12.630 ± 0.014	13.069 ± 0.039	...	-0.491	-0.480	-0.452	-0.040	...	-1.590 ± 0.040
V54	13:26:23.54	-47:18:47.7	RRab	0.773	13.294 ± 0.005	13.026 ± 0.005	12.968 ± 0.004	12.906 ± 0.014	...	0.019	0.020	0.049	-0.050	...	-1.850 ± 0.020
V56	13:25:55.53	-47:37:44.1	RRab	0.568	13.690 ± 0.003	13.462 ± 0.006	13.383 ± 0.005	...	13.385 ± 0.015	0.137	0.153	0.144	...	0.059	-1.420 ± 0.150
V57	13:27:49.38	-47:36:50.5	RRab	0.794	13.256 ± 0.004	13.091 ± 0.005	12.897 ± 0.004	0.006	0.112	0.006	-2.110 ± 0.140
V58	13:26:13.05	-47:24:03.0	RRc	0.370	13.676 ± 0.005	13.517 ± 0.005	13.426 ± 0.006	...	13.575 ± 0.014	0.071	0.085	0.066	...	0.160	-1.640 ± 0.240
V59	13:26:18.43	-47:29:46.7	RRab	0.519	13.740 ± 0.007	13.433 ± 0.012	13.408 ± 0.010	...	13.428 ± 0.022	0.104	0.033	0.075	-0.002	-1.130 ± 0.280	
V62	13:26:26.59	-47:27:55.4	RRab	0.620	13.473 ± 0.008	13.105 ± 0.021	13.098 ± 0.015	13.087 ± 0.014	...	-0.001	-0.118	-0.050	-0.084	...	-1.810 ± 0.290
V63	13:25:07.96	-47:36:54.1	RRab	0.826	13.237 ± 0.005	12.876 ± 0.005	12.881 ± 0.003	0.022	-0.065	0.030	-1.940 ± 0.090
V64	13:26:02.22	-47:36:19.2	RRc	0.344	13.647 ± 0.004	13.461 ± 0.006	13.419 ± 0.006	...	13.429 ± 0.012	-0.024	-0.047	-0.017	...	-0.057	-1.640 ± 0.230
V66	13:26:33.08	-47:22:25.2	RRc	0.407	13.548 ± 0.003	13.382 ± 0.006	13.274 ± 0.006	13.274 ± 0.007	...	0.032	0.051	0.017	-0.033	...	-1.880 ± 0.340
V67	13:26:28.62	-47:18:46.9	RRab	0.564	13.657 ± 0.004	13.422 ± 0.004	13.356 ± 0.004	13.441 ± 0.016	...	0.097	0.107	0.111	0.179	...	-1.220 ± 0.020

Continued on next page

Table A1 - *Continued from previous page*

ID	RA (J2000)	Dec (J2000)	Mode	P (days)	J mag	H mag	K_s mag	[3.6] mag	[4.5] mag	ΔJ	ΔH	ΔK_s	$\Delta [3.6]$	$\Delta [4.5]$	[Fe/H]
V68	13:26:12.80	-47:19:35.7	RRc	0.535	13.271 ± 0.006	13.024 ± 0.004	12.977 ± 0.004	13.068 ± 0.013	...	0.005	-0.018	0.010	0.123	...	-1.790 ± 0.010
V69	13:25:11.02	-47:37:33.5	RRab	0.653	13.128 ± 0.004	0.035	-1.700 ± 0.140
V70	13:27:27.76	-47:33:42.7	RRc	0.391	13.535 ± 0.004	13.293 ± 0.008	13.260 ± 0.006	-0.020	-0.082	-0.042	-2.090 ± 0.230
V71	13:27:08.08	-47:27:51.6	RRc	0.358	13.597 ± 0.006	13.305 ± 0.018	13.339 ± 0.010	...	13.135 ± 0.009	-0.039	-0.163	-0.057	...	-0.314	-1.760 ± 0.280
V72	13:27:33.11	-47:16:22.9	RRc	0.385	13.561 ± 0.003	13.358 ± 0.005	13.321 ± 0.004	-0.009	-0.033	0.001	-1.480 ± 0.220
V73	13:25:53.75	-47:16:10.8	RRab	0.575	13.508 ± 0.005	13.284 ± 0.005	13.227 ± 0.005	-0.034	-0.014	0.001	-1.680 ± 0.090
V74	13:27:07.22	-47:17:33.9	RRab	0.503	13.680 ± 0.002	13.490 ± 0.005	13.446 ± 0.004	0.017	0.061	0.082	-2.050 ± 0.360
V75	13:27:19.70	-47:18:46.5	RRc	0.422	13.418 ± 0.003	13.194 ± 0.008	13.144 ± 0.007	-0.066	-0.099	-0.075	-1.670 ± 0.020
V76	13:26:57.23	-47:20:07.7	RRc	0.338	13.639 ± 0.003	13.522 ± 0.005	13.454 ± 0.006	-0.049	-0.006	-0.003	-1.630 ± 0.130
V77	13:27:20.89	-47:22:05.6	RRc	0.426	13.479 ± 0.004	13.297 ± 0.008	13.233 ± 0.006	0.004	0.014	0.024	-1.930 ± 0.110
V79	13:28:24.99	-47:29:25.2	RRab	0.608	13.412 ± 0.003	13.199 ± 0.005	13.148 ± 0.004	-0.080	-0.043	-0.019	-1.560 ± 0.180
V81	13:27:36.68	-47:24:48.3	RRc	0.389	13.548 ± 0.004	13.336 ± 0.010	13.297 ± 0.007	13.307 ± 0.011	...	-0.010	-0.042	-0.009	-0.060	...	-1.950 ± 0.060
V82	13:27:35.61	-47:26:30.3	RRc	0.336	13.589 ± 0.005	13.351 ± 0.007	13.302 ± 0.005	13.533 ± 0.026	...	-0.106	-0.184	-0.162	-0.030	...	-1.750 ± 0.010
V83	13:27:08.42	-47:21:34.1	RRc	0.357	13.610 ± 0.003	13.477 ± 0.007	13.376 ± 0.006	-0.028	0.006	-0.024	-1.460 ± 0.220
V84	13:24:47.45	-47:29:56.5	RRab	0.580	...	12.885 ± 0.005	12.808 ± 0.005	-0.404	-0.409	-1.650 ± 0.100
V85	13:25:06.49	-47:23:34.0	RRab	0.743	13.358 ± 0.003	0.048	-2.090 ± 0.310
V86	13:27:15.19	-47:26:11.1	RRab	0.648	13.463 ± 0.006	13.162 ± 0.017	13.084 ± 0.012	13.116 ± 0.019	...	0.029	-0.018	-0.018	-0.012	...	-2.020 ± 0.010
V87	13:26:57.47	-47:25:35.4	RRc	0.396	13.393 ± 0.016	13.113 ± 0.024	13.071 ± 0.031	13.043 ± 0.007	...	-0.150	-0.247	-0.217	-0.302	...	-1.620 ± 0.190
V88	13:26:55.91	-47:25:16.3	RRab	0.690	12.710 ± 0.008	12.405 ± 0.016	12.172 ± 0.017	12.338 ± 0.015	...	-0.667	-0.712	-0.865	-0.728	...	-1.850 ± 0.230
V89	13:26:45.98	-47:26:01.0	RRc	0.374	13.746 ± 0.009	13.663 ± 0.020	13.436 ± 0.015	13.599 ± 0.013	...	0.151	0.242	0.088	0.179	...	-1.620 ± 0.100
V90	13:26:45.76	-47:26:23.4	RRab	0.603	13.517 ± 0.008	13.159 ± 0.041	13.111 ± 0.021	0.018	-0.091	-0.064	-1.980 ± 0.420
V91	13:26:50.61	-47:26:15.6	RRab	0.895	13.058 ± 0.006	12.737 ± 0.012	12.729 ± 0.011	14.127 ± 0.034	...	-0.083	-0.124	-0.037	1.314	...	-1.670 ± 0.130
V94	13:25:57.06	-47:22:46.1	RRc	0.254	14.101 ± 0.007	13.959 ± 0.006	13.878 ± 0.008	13.975 ± 0.005	...	0.150	0.127	0.116	0.041	...	-1.130 ± 0.110
V95	13:25:24.95	-47:28:53.2	RRc	0.405	13.507 ± 0.004	13.283 ± 0.005	13.268 ± 0.005	...	13.236 ± 0.009	-0.015	-0.054	0.004	...	-0.089	-2.060 ± 0.550
V96	13:26:39.31	-47:27:03.0	RRab	0.625	13.043 ± 0.027	-0.121	...	-1.370 ± 0.500
V97	13:27:08.49	-47:25:30.9	RRab	0.692	13.326 ± 0.003	13.157 ± 0.008	13.053 ± 0.006	13.077 ± 0.025	...	-0.049	0.042	0.019	0.013	...	-1.760 ± 0.010
V98	13:27:05.85	-47:26:56.5	RRc	0.281	13.882 ± 0.010	13.633 ± 0.019	13.654 ± 0.015	13.271 ± 0.012	13.592 ± 0.022	0.022	-0.093	-0.002	-0.532	-0.099	-1.180 ± 0.120
V99	13:27:02.16	-47:27:48.8	RRab	0.766	13.079 ± 0.006	12.632 ± 0.016	12.666 ± 0.014	...	12.667 ± 0.023	-0.204	-0.383	-0.262	...	-0.321	-1.880 ± 0.040
V100	13:27:04.04	-47:27:33.4	RRab	0.553	13.596 ± 0.009	13.225 ± 0.022	13.213 ± 0.019	0.018	-0.111	-0.054	-1.770 ± 0.140
V101	13:27:30.24	-47:29:51.0	RRc	0.341	13.714 ± 0.005	13.509 ± 0.009	13.441 ± 0.007	0.034	-0.010	-0.007	-2.100 ± 0.320
V102	13:27:22.11	-47:30:12.3	RRab	0.691	13.340 ± 0.003	13.053 ± 0.006	13.002 ± 0.006	13.122 ± 0.031	13.530 ± 0.054	-0.035	-0.062	-0.032	0.057	0.426	-1.900 ± 0.270
V103	13:27:14.29	-47:28:36.3	RRc	0.329	13.626 ± 0.005	13.433 ± 0.012	13.382 ± 0.010	-0.088	-0.124	-0.104	-2.100 ± 0.170
V104	13:28:07.76	-47:33:44.9	RRab	0.867	13.852 ± 0.028	14.302 ± 0.054	13.868 ± 0.041	0.681	1.409	1.067	-2.050 ± 0.180
V105	13:27:46.02	-47:32:43.9	RRc	0.335	13.777 ± 0.004	13.625 ± 0.006	13.539 ± 0.005	0.082	0.088	0.074	-1.390 ± 0.180
V106	13:26:59.19	-47:28:12.5	RRab	0.570	13.574 ± 0.008	13.281 ± 0.024	13.230 ± 0.015	13.277 ± 0.021	...	0.024	-0.025	-0.005	0.023	...	-1.790 ± 0.170
V107	13:27:14.05	-47:30:57.9	RRab	0.514	13.603 ± 0.005	13.352 ± 0.011	13.327 ± 0.009	-0.035	-0.056	-0.015	-1.530 ± 0.110
V108	13:27:04.71	-47:29:25.7	RRab	0.594	13.471 ± 0.014	13.011 ± 0.026	13.062 ± 0.026	...	13.082 ± 0.016	-0.041	-0.254	-0.130	...	-0.194	-1.770 ± 0.310
V109	13:27:01.56	-47:29:36.6	RRab	0.744	13.287 ± 0.006	13.075 ± 0.016	12.997 ± 0.010	...	12.790 ± 0.020	-0.022	0.032	0.039	...	-0.232	-1.720 ± 0.010
V110	13:27:02.08	-47:30:06.6	RRc	0.332	13.804 ± 0.006	13.759 ± 0.014	13.594 ± 0.010	...	12.752 ± 0.009	0.100	0.212	0.118	...	-0.771	-2.330 ± 0.290
V111	13:26:49.03	-47:28:40.4	RRab	0.763	13.236 ± 0.007	12.907 ± 0.025	12.869 ± 0.017	12.998 ± 0.020	...	-0.050	-0.112	-0.064	0.029	...	-1.850 ± 0.030
V112	13:26:54.28	-47:30:23.2	RRab	0.474	13.689 ± 0.005	13.396 ± 0.015	13.442 ± 0.009	-0.027	-0.092	0.017	-2.020 ± 0.260
V113	13:26:56.34	-47:31:47.6	RRab	0.573	13.598 ± 0.006	13.413 ± 0.015	13.272 ± 0.009	0.053	0.112	0.043	-1.850 ± 0.340
V114	13:26:50.12	-47:30:21.1	RRab	0.675	12.545 ± 0.019	12.395 ± 0.024	12.077 ± 0.032	12.406 ± 0.013	12.083 ± 0.011	-0.852	-0.744	-0.982	-0.682	-1.048	-1.490 ± 0.060
V115	13:26:12.30	-47:34:17.5	RRab	0.630	13.408 ± 0.003	13.191 ± 0.005	13.117 ± 0.004	...	13.081 ± 0.011	-0.051	-0.015	-0.013	...	-0.128	-2.090 ± 0.020
V116	13:26:35.50	-47:28:07.0	RRab	0.720	12.719 ± 0.014	12.259 ± 0.021	12.098 ± 0.021	13.073 ± 0.040	...	-0.620	-0.816	-0.894	0.048	...	-1.170 ± 0.140
V117	13:26:19.91	-47:29:21.0	RRc	0.422	13.486 ± 0.006	13.281 ± 0.012	13.207 ± 0.009	...	13.078 ± 0.012	0.001	-0.013	-0.014	...	-0.207	-1.880 ± 0.250
V118	13:26:40.56	-47:30:19.1	RRab	0.612	13.401 ± 0.006	13.130 ± 0.016	13.013 ± 0.014	12.986 ± 0.022	13.042 ± 0.008	-0.085	-0.107	-0.149	-0.199	-0.201	-1.990 ± 0.150
V119	13:26:38.29	-47:31:18.0	RRc	0.306	13.853 ± 0.006	13.783 ± 0.012	13.634 ± 0.008	13.757 ± 0.011	13.673 ± 0.056	0.073	0.149	0.070	0.070	0.068	-1.800 ± 0.100
V120	13:26:25.52	-47:32:48.6	RRab	0.549	13.555 ± 0.014	13.116 ± 0.023	13.155 ± 0.027	13.205 ± 0.028	13.195 ± 0.015	-0.030	-0.228	-0.120	-0.086	-0.172	-1.510 ± 0.180
V121	13:26:28.17	-47:31:50.5	RRc	0.304	13.745 ± 0.005	13.659 ± 0.009	13.536 ± 0.008	13.565 ± 0.004	...	-0.040	0.019	-0.033	-0.130	...	-1.660 ± 0.090
V122	13:26:30.31	-47:33:02.2	RRab	0.635	13.384 ± 0.005	13.147 ± 0.012	13.086 ± 0.007	13.257 ± 0.024	13.484 ± 0.035	-0.068	-0.053	-0.037	0.109	0.284	-2.070 ± 0.310
V123	13:26:51.17	-47:37:13.2	RRc	0.475	13.474 ± 0.004	13.265 ± 0.005	13.177 ± 0.005	0.099	0.097	0.083	-1.840 ± 0.010
V124	13:26:54.49	-47:39:07.5	RRc	0.332	13.718 ± 0.004	13.532 ± 0.005	13.497 ± 0.007	0.013	-0.015	0.021	-1.490 ± 0.230
V125	13:26:48.92	-47:41:03.7	RRab	0.593	13.481 ± 0.004	13.229 ± 0.005	13.182 ± 0.004	-0.034	-0.038	-0.012	-1.860 ± 0.020
V126	13:28:08.03	-47:40:46.7	RRc	0.342	13.648 ± 0.003	13.488 ± 0.005	13.375 ± 0.005	-0.030	-0.029	-0.069	-1.470 ± 0.130
V127	13:25:19.36	-47:28:37.6	RRc	0.305	13.583 ± 0.005	...	13.						

Table A1 - *Continued from previous page*

ID	RA (J2000)	Dec (J2000)	Mode	P (days)	J mag	H mag	K_s mag	[3.6] mag	[4.5] mag	ΔJ	ΔH	ΔK_s	$\Delta [3.6]$	$\Delta [4.5]$	[Fe/H]
V135	13:26:28.14	-47:29:17.6	RRab	0.633	13.552 ± 0.051	...	12.672 ± 0.061	10.182 ± 0.015	...	0.096	-0.455	-2.969	...	-1.690 ± 0.390	
V136	13:26:31.09	-47:27:40.5	RRc	0.392	13.514 ± 0.012	13.010 ± 0.048	13.221 ± 0.016	-0.038	-0.362	-0.078	...	-1.810 ± 0.270	
V137	13:26:31.55	-47:27:04.3	RRc	0.334	13.774 ± 0.006	13.705 ± 0.012	13.479 ± 0.009	13.717 ± 0.009	...	0.076	0.165	0.010	0.147	...	-1.340 ± 0.180
V139	13:26:37.76	-47:27:35.2	RRab	0.677	13.111 ± 0.005	12.860 ± 0.013	12.731 ± 0.010	12.975 ± 0.016	...	-0.284	-0.277	-0.326	-0.110	...	-1.650 ± 0.060
V140	13:26:42.16	-47:30:07.1	RRab	0.620	13.022 ± 0.011	12.576 ± 0.030	12.667 ± 0.022	12.807 ± 0.013	...	-0.452	-0.647	-0.481	-0.365	...	-1.740 ± 0.150
V141	13:26:40.91	-47:29:27.9	RRab	0.697	13.338 ± 0.007	12.954 ± 0.028	12.932 ± 0.013	-0.030	-0.153	-0.094	...	-1.980 ± 0.340	
V142	13:26:42.67	-47:28:42.7	RRc	0.376	13.175 ± 0.021	12.589 ± 0.031	12.580 ± 0.036	12.998 ± 0.007	...	-0.415	-0.827	-0.764	-0.416	...	-1.830 ± 0.240
V143	13:26:42.64	-47:27:28.8	RRab	0.821	13.319 ± 0.019	12.263 ± 0.069	12.150 ± 0.024	0.099	-0.683	-0.707	...	-2.090 ± 0.140	
V144	13:26:43.06	-47:28:17.9	RRab	0.835	13.190 ± 0.005	12.938 ± 0.018	12.857 ± 0.012	12.955 ± 0.015	...	-0.014	0.009	0.018	0.075	...	-1.910 ± 0.120
V145	13:26:51.26	-47:31:08.6	RRc	0.374	13.459 ± 0.014	13.082 ± 0.027	13.142 ± 0.028	-0.136	-0.339	-0.206	...	-1.770 ± 0.070	
V146	13:26:52.87	-47:29:27.9	RRab	0.633	13.521 ± 0.009	13.907 ± 0.077	13.093 ± 0.023	12.623 ± 0.034	...	0.065	0.704	-0.033	-0.527
V147	13:27:15.86	-47:31:09.2	RRc	0.422	13.403 ± 0.004	13.038 ± 0.012	13.089 ± 0.006	-0.080	-0.254	-0.130	...	-1.860 ± 0.140	
V149	13:27:32.94	-47:13:43.6	RRab	0.683	13.389 ± 0.004	13.166 ± 0.010	13.045 ± 0.007	0.002	0.037	-0.003	...	-1.360 ± 0.240	
V150	13:27:40.21	-47:36:00.1	RRab	0.899	13.084 ± 0.006	12.824 ± 0.007	12.721 ± 0.005	-0.054	-0.033	-0.040	...	-1.970 ± 0.340	
V151	13:28:25.40	-47:16:00.2	RRab	0.408	13.503 ± 0.004	13.319 ± 0.006	13.274 ± 0.005	-0.350	-0.317	-0.308	...	-1.460 ± 0.240	
V153	13:26:49.69	-47:26:23.7	RRc	0.386	13.659 ± 0.007	13.573 ± 0.022	13.397 ± 0.014	13.345 ± 0.007	...	0.094	0.186	0.082	-0.033	...	-1.550 ± 0.190
V154	13:27:03.15	-47:30:32.6	RRc	0.322	13.632 ± 0.005	13.470 ± 0.011	13.385 ± 0.012	...	13.714 ± 0.015	-0.099	-0.109	-0.122	...	0.162	-1.550 ± 0.030
V155	13:26:53.63	-47:24:42.5	RRc	0.414	13.291 ± 0.014	12.963 ± 0.024	12.986 ± 0.026	12.971 ± 0.009	...	-0.211	-0.350	-0.254	-0.315	...	-1.640 ± 0.090
V156	13:26:47.92	-47:31:52.5	RRc	0.359	13.464 ± 0.010	13.144 ± 0.022	13.182 ± 0.022	...	14.313 ± 0.017	-0.169	-0.320	-0.210	...	0.868	-1.570 ± 0.010
V157	13:26:46.49	-47:27:17.5	RRc	0.406	13.625 ± 0.009	13.674 ± 0.029	13.412 ± 0.019	13.623 ± 0.013	...	0.106	0.340	0.151	0.311	...	-1.670 ± 0.100
V158	13:26:45.34	-47:30:40.2	RRc	0.367	13.660 ± 0.007	13.516 ± 0.030	13.484 ± 0.014	13.181 ± 0.008	...	0.048	0.076	0.115	-0.264	...	-1.410 ± 0.040
V163	13:25:49.42	-47:20:21.5	RRc	0.313	13.779 ± 0.005	13.583 ± 0.005	13.560 ± 0.007	0.020	-0.025	0.022	...	-1.330 ± 0.270	
V165	13:26:39.44	-47:26:56.1	RRab	0.501	13.776 ± 0.015	13.645 ± 0.030	13.487 ± 0.028	13.248 ± 0.015	...	0.109	0.211	0.118	-0.132
V166	13:26:46.00	-47:26:15.3	RRc	0.340	13.557 ± 0.009	13.274 ± 0.021	13.322 ± 0.018	13.231 ± 0.005	...	-0.125	-0.248	-0.128	-0.315
V168	13:25:52.78	-47:32:02.9	RRc	0.321	14.186 ± 0.004	14.011 ± 0.006	13.969 ± 0.005	0.452	0.429	0.458
V169	13:27:20.47	-47:23:59.1	RRc	0.319	13.807 ± 0.004	13.770 ± 0.006	13.674 ± 0.007	13.643 ± 0.016	...	0.066	0.181	0.155	0.012	...	-1.670 ± 0.190
V184	13:27:28.50	-47:31:35.4	RRc	0.303	13.781 ± 0.003	13.640 ± 0.008	13.539 ± 0.006	-0.007	-0.003	-0.033
V185	13:26:04.13	-47:21:45.0	RRc	0.333	13.714 ± 0.005	13.582 ± 0.005	13.514 ± 0.007	...	13.786 ± 0.013	0.013	0.039	0.042	...	0.266	...
V261	13:27:15.41	-47:21:29.5	RRc	0.403	13.432 ± 0.003	13.250 ± 0.005	13.132 ± 0.006	-0.096	-0.093	-0.139	...	-1.520 ± 0.350	
V263	13:26:13.13	-47:26:09.7	RRab	1.012	13.160 ± 0.005	12.898 ± 0.005	12.754 ± 0.005	12.777 ± 0.010	12.971 ± 0.011	0.129	0.157	0.115	0.084	0.298	-1.750 ± 0.190
V264	13:26:39.66	-47:30:28.2	RRc	0.321	13.878 ± 0.008	13.907 ± 0.047	13.615 ± 0.015	15.088 ± 0.024	...	0.143	0.325	0.105	1.467
V265	13:26:30.22	-47:28:45.2	RRc	0.422	13.495 ± 0.006	13.341 ± 0.014	13.236 ± 0.009	0.011	0.047	0.016	...	-2.020 ± 0.290	
V266	13:26:39.65	-47:28:01.7	RRc	0.352	13.451 ± 0.016	13.201 ± 0.030	13.152 ± 0.031	-0.199	-0.284	-0.261	
V267	13:26:40.23	-47:26:35.8	RRc	0.316	13.418 ± 0.018	12.958 ± 0.029	12.923 ± 0.030	13.023 ± 0.006	...	-0.332	-0.643	-0.606	-0.622	...	-1.640 ± 0.630
V268	13:26:35.16	-47:26:10.9	RRab	0.813	13.105 ± 0.012	12.387 ± 0.021	12.595 ± 0.021	-0.124	-0.569	-0.272	...	-1.780 ± 0.240	
V270	13:26:56.57	-47:30:05.7	RRc	0.313	13.650 ± 0.010	13.427 ± 0.024	13.428 ± 0.020	...	13.469 ± 0.014	-0.109	-0.182	-0.110	...	-0.113	...
V271	13:26:47.13	-47:30:04.1	RRc	0.443	13.119 ± 0.015	12.566 ± 0.034	12.620 ± 0.032	12.887 ± 0.008	...	-0.320	-0.675	-0.548	-0.308	...	-1.820 ± 0.210
V272	13:26:42.95	-47:25:56.6	RRc	0.311	13.817 ± 0.006	13.644 ± 0.012	13.573 ± 0.009	13.630 ± 0.006	...	0.054	0.029	0.029	-0.033
V273	13:26:54.34	-47:27:08.7	RRc	0.367	13.605 ± 0.011	13.529 ± 0.052	13.344 ± 0.030	-0.007	0.089	-0.025	
V274	13:26:43.73	-47:22:48.2	RRc	0.311	13.831 ± 0.003	13.784 ± 0.007	13.660 ± 0.006	14.267 ± 0.038	...	0.066	0.168	0.115	0.601
V275	13:26:49.75	-47:27:37.3	RRc	0.378	13.491 ± 0.012	13.331 ± 0.049	13.161 ± 0.024	-0.095	-0.079	-0.177	...	-1.680 ± 0.360	
V276	13:27:16.51	-47:33:17.6	RRc	0.308	13.728 ± 0.006	13.629 ± 0.013	13.537 ± 0.007	-0.046	0.002	-0.020	
V277	13:26:59.97	-47:27:29.2	RRc	0.352	13.611 ± 0.007	13.353 ± 0.018	13.359 ± 0.012	13.449 ± 0.013	...	-0.041	-0.133	-0.056	-0.054
V280	13:27:09.33	-47:23:05.7	RRc	0.282	13.953 ± 0.003	13.950 ± 0.008	13.826 ± 0.008	0.097	0.228	0.174	
V285	13:25:40.20	-47:34:48.4	RRc	0.329	13.689 ± 0.005	13.510 ± 0.008	13.506 ± 0.004	-0.024	-0.047	0.020	
V288	13:28:10.32	-47:23:47.8	RRc	0.296	13.812 ± 0.003	13.740 ± 0.005	13.659 ± 0.006	0.001	0.070	0.059	
V289	13:28:03.68	-47:21:27.9	RRc	0.308	13.745 ± 0.004	13.625 ± 0.004	13.601 ± 0.006	13.651 ± 0.006	...	-0.029	-0.002	0.045	-0.027	...	
V291	13:26:38.52	-47:33:28.0	RRc	0.334	13.677 ± 0.005	13.527 ± 0.013	13.446 ± 0.008	-0.022	-0.014	-0.023	
NV339	13:26:29.67	-47:29:51.8	RRc	0.301	13.740 ± 0.006	13.419 ± 0.016	13.440 ± 0.009	...	13.635 ± 0.034	-0.054	-0.231	-0.139	...	0.015	
NV340	13:26:38.95	-47:27:32.5	RRc	0.302	13.490 ± 0.014	13.094 ± 0.025	13.091 ± 0.026	13.307 ± 0.005	...	-0.302	-0.554	-0.487	-0.399	...	
NV341	13:26:54.61	-47:28:47.7	RRc	0.306	13.769 ± 0.013	13.335 ± 0.023	13.370 ± 0.017	-0.011	-0.298	-0.193	...	-1.800 ± 0.590	
NV342	13:27:18.69	-47:28:22.9	RRc	0.308	13.683 ± 0.008	13.361 ± 0.014	13.422 ± 0.014	-0.089	-0.265	-0.133	...	-1.730 ± 0.550	
NV343	13:26:47.79	-47:29:36.8	RRc	0.310	13.652 ± 0.013	13.469 ± 0.033	13.443 ± 0.023	13.181 ± 0.008	...	-0.115	-0.150	-0.105	-0.488	...	
NV344	13:26:38.09	-47:24:44.7	RRc	0.314	13.790 ± 0.010	13.763 ± 0.043	13.650 ± 0.017	0.034	0.156	0.114	...	-1.540 ± 0.540	
NV346	13:26:46.93	-47:28:14.1	RRc	0.328	13.673 ± 0.010	12.696 ± 0.034	13.406 ± 0.021	-0.044	-0.865	-0.084	...	-1.680 ± 0.270	
NV347	13:26:50.88	-47:27:46.2	RRc	0.329	12.673 ± 0.045	-0.860	...	
NV349	13:26:51.80	-47:27:43.9	RRc	0.364	13.759 ± 0.061	0.140	
NV350	13:26:56.40	-47:30:50.2	RRc	0.379	13.219 ± 0.017	13.029 ± 0.030	12.764 ± 0.035	...	12.980 ± 0.016	-0.363	-0.378	-0.570	...	-0.411	-1.470 ± 0.400
NV352	13:26														

Table A1 - *Continued from previous page*

ID	RA (J2000)	Dec (J2000)	Mode	P (days)	J mag	H mag	K_s mag	[3.6] mag	[4.5] mag	ΔJ	ΔH	ΔK_s	$\Delta [3.6]$	$\Delta [4.5]$	[Fe/H]
NV354	13:26:38.63	-47:25:09.9	RRc	0.419	13.521 \pm 0.005	13.313 \pm 0.015	13.281 \pm 0.011	13.169 \pm 0.011	...	0.031	0.013	0.054	-0.099	...	-1.750 \pm 0.230
NV357	13:26:17.77	-47:30:23.4	RRc	0.298	13.694 \pm 0.008	13.476 \pm 0.018	13.489 \pm 0.013	13.725 \pm 0.008	...	-0.111	-0.187	-0.103	0.002	...	-1.660 \pm 0.990
NV366	13:26:41.56	-47:31:42.0	RRab	1.000	12.802 \pm 0.009	12.070 \pm 0.020	12.311 \pm 0.015	12.628 \pm 0.018	12.023 \pm 0.038	-0.240	-0.683	-0.341	-0.077	-0.664	-1.630 \pm 0.140
NV399	13:26:29.53	-47:30:02.6	RRc	0.310	13.670 \pm 0.011	13.446 \pm 0.026	13.452 \pm 0.019	-0.098	-0.174	-0.098	-1.720 \pm 0.670

This paper has been typeset from a T_EX/L_AT_EX file prepared by the author.